An Analytical Relationship of Concentration-Dependent Interfacial Solute Distribution Coefficient for Aqueous Layer Freeze Concentration

Xiao Dong Chen and Winston Duo Wu
Suzhou Key Laboratory of Green Chemical Engineering, School of Chemical and Environmental Engineering, College of Chemistry, Chemical Engineering and Materials Science, Soochow University, Suzhou Industrial Park, Jiangsu Province, China

Ping Chen
Nutrition and Health Research Institute, China Oil and Foodstuffs corporation (COFCO), Beijing, China

DOI 10.1002/aic.14722
Published online January 20, 2015 in Wiley Online Library (wileyonlinelibrary.com)

Freeze concentration (FC) is a subzero temperature solute concentration procedure, favoring the retention of high quality compounds such as food ingredients and biological materials. It is known that modeling solute inclusion in the ice layers or ice crystals formed in a convective environment requires the solute distribution coefficient function. The fluid flow velocity, ice-growth rate and solute concentration are influential on this function. Some literature has reported certain expressions of the function, which are relatively complex. Here, an explicit format of this function has been derived for single solute system, and found to be satisfactory in correlating a wide range of experimental data on sucrose solutions for both the controlled flow layer crystallization process (flow in between two cooling plates) as well as the falling film crystallization process. This expression has captured the fundamental aspects of mass transfer, and it is relatively simple which should be very useful for correlating FC parameters and for simulating the layer FC processes. © 2015 American Institute of Chemical Engineers *AIChE J*, 61: 1334–1344, 2015
Keywords: freeze concentration, interfacial distribution coefficient, controlled flow suspension crystallizer, falling film crystallizer

Introduction

Freeze concentration (FC) is a physical solute concentration process, which involves the fractional crystallization of water and subsequent removal of the ice, resulting in an enriched solution.[1] Because it is a subzero temperature processing method, it is recognized as a beneficial alternative to evaporative concentration method of heat sensitive materials such as food and biological materials.

Figure 1 shows two basic modes of FC operations. Two subsystems for (b), that is, (b1) and (b2), are also illustrated. In this study, we focus on (b1) and (b2). These two are popular testing approaches in flow systems for FC[2–6] though the geometry may vary. In a FC process, impurities may be entrapped in solid ice matrices, which can be separated later from the ice phase during the formation of ice crystals. The entrapped materials may be what one wants for certain purposes. However, it is most often in FC operations that the impurity in ice should be kept minimal to minimize the loss of valuable solutes in food or in bioactive materials.

In recent years, FC has also been researched on to apply it as an alternative for seawater desalination and wastewater treatment processes.[7,8] Freeze desalination has some advantages when compared with other methods. It is argued that one of the main advantages of freeze desalination systems is its energy consumption. It requires only 420 kJ kg^{-1} of energy to remove salt and produce 1 kg of fresh water largely due to the low latent heat of freezing. In addition to that, freeze desalination system is corrosive resistance and can operate for a long time with little maintenance.[7,9]

Interestingly, it has also been investigated as an enhancement process for bioactive compounds in aqueous extract. For instance, the effects of FC of aqueous extract of mate leaves on the content of bioactive components and antioxidant activity of the concentrated fluid and the ice have been looked at in a FC process.[10] Multistage FC process was used in laboratory and the concentrated fluid shows increasing phenolic compounds in all the FC stages. The isolated phenolic compounds detected by HPLC, such as chlorogenic acid, 3,5-dicaffeoylquinic acid, caffeic-acid, *p*-coumaric acid, 3,4-dihidroxibenzoic acid, and gallic acid, all improve substantially in all FC stages. The methylxanthines caffeine and theobromine contents have also been found to increase significantly with the application of the FC procedure.

Another recent study has suggested that the solute inclusion in NaCl system is affected by the directional growth of the ice on cooled surface.[11] It is expected that the freezing, microstructure and solute inclusion is interactive, and the relationships are still subjects to be investigated in near future.

Correspondence concerning this article should be addressed to Xiao Dong Chen at xdchen@suda.edu.cn or Winston Duo Wu at duo.wu@suda.edu.cn

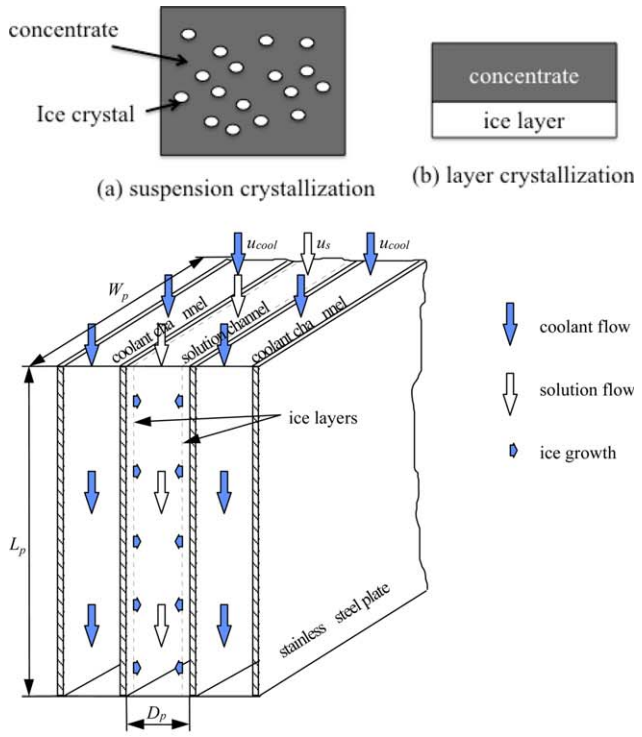

Figure 1. Basic freeze concentration (or freeze crystallization) processes (a) creating ice crystals suspended in a solution and growing them till large to be separated; (b) creating an ice layer that has some purity so the remaining liquid is a concentrated one; (b1) and (b2) are a couple of illustrative options of layer crystallization process that can also produce enriched concentrates: one is a saturated flow in between two plates cooled from both sides and one has liquid flow naturally fall along a cooled surface.

[Color figure can be viewed in the online issue, which is available at wileyonlinelibrary.com.]

Distribution coefficients

As far as separation and purification is concerned, from process engineering prospective, solute inclusion in the ice formed in FC is a key subject of interest. The process has been characterized using a distribution coefficient which is thus an extremely important parameter reflecting the efficiency of the process. The distribution coefficient, a thermodynamic parameter for describing the impurity distribution in solid and liquid phases during solidification, is defined as the ratio of the impurity concentration in the crystal and in the mother solution expressed in weight fractions.[12–14] Three distribution coefficients have been defined previously.[13,14] They are the equilibrium distribution coefficient K_{eq}, the interfacial distribution coefficient K_i, and the effective distribution coefficient K, respectively

$$K_{eq}=\frac{C_S}{C_L} \quad v=0 \tag{1}$$

$$K=\frac{C_S}{C_L} \quad v\neq 0 \tag{2}$$

$$K_i=\frac{C_S}{C_{L.i}} \quad v\neq 0 \tag{3}$$

where C_S is the concentration of solute in the solid, C_L in the bulk liquid, and $C_{L,i}$ in the liquid adjacent to the interface. K_{eq} denotes the equilibrium values and both K_i and K denote the nonequilibrium distribution coefficients due to both thermodynamic and the kinetic factors. v is the linear fluid velocity at the crystallizing surface.

The purity of the crystal is not only determined by the thermodynamic (or equilibrium) distribution coefficient, but also by the growth mechanism. Due to the kinetic effects, impurities may be included in the crystal lattice both on a micro- and a macroscale.[15] On a microscale, molecules of the impurities may be incorporated in the lattice itself or in the dislocations of the crystal. The incorporation of foreign molecules into the crystal lattice may be easier as the volumes of the foreign molecules are similar to those of the main crystallizing compound.[16] On a microscale, the mother liquor with its contained impurities may be included inside crystal imperfections or may be trapped in the agglomerates of crystals. The contribution of the kinetic effects to the purity of the crystals or crystal layers will depend on the configuration of the crystallizer and the process conditions during the crystal growth.

The contribution of the interfacial kinetics may be limited either by a relatively low enthalpy of melting or a high driving force.[16] A low melt enthalpy means that the differences in lattice energy of the main compound molecules and the impurity molecules, which resemble the main compound molecules, are small. The selectivity may easily decrease due to kinetic effects. If the driving force is increasing to relatively large values (i.e., a large supersaturation/supercooling), the differences in attachment energy between the main compound molecules and the impurity molecules become relatively less important. The selectivity is decreased again. Moreover, the concentration of impurities at the interface may strongly increase due to mass transfer limitations, increasing the incorporation tendency of the impurities. This will especially be the case, when a large growth rate is established by high supersaturation/supercooling. Therefore, it will be clear that crystallization under condition of dendritic growth will result in a poor selectivity due to the large amount of melt inclusions.

Chernov considered impurity incorporation in crystals from a kinetic viewpoint[17,18] and as a random walk problem.[19] Several researchers such as Baralis[20] and Baur[21] calculated nonequilibrium distribution coefficients by the methods of nonequilibrium thermodynamics. Crystallization kinetics of binary melts was treated from the absolute reaction rate theory viewpoint by Kirwan and Pigford.[22] Baker[23] observed solute trapping of zinc when zinc–cadmium alloys were rapidly solidified. They concluded that only the theory of Chernov[17] could explain the results. Chernov[24] discussed the mechanism and the kinetics of the trapping of impurities by the surface of a layer-wise-growing crystal, and also the subsequent relaxation processes. He thought that a new layer laid by a step buries the impurity atoms of the surface layer, transferring them from a position in the surface to a position in the bulk. The concentrations of an impurity in the surface and in the bulk are different, and therefore, the amount of impurity in just buried regions of the crystal bulk will not be equilibrium. A situation may occur on the step: building up new atomic rows during the motion of kinks and burying the impurity atoms in the step rise lead to a nonequilibrium concentration of the impurity in the surface layer.

If the growth rate is high enough, the crystal traps the impurity in an amount differing from the equilibrium amount, and there is no time for subsequent relaxation to take place. The result is nonequilibrium trapping and the appearance of metastable structures (diffusionless crystallization). However, Arkenbout[15] pointed out that Chernov's models are not yet available for organic molecules.

Models of distribution coefficient

The practical systems are perhaps always operated under nonequilibrium conditions. The effective distribution coefficient is normally used to describe the distribution of solute between the liquid and solid phases. Burton et al.[25] expressed a relationship between K and K_{eq} according to the mass transfer boundary layer theory

$$K=\frac{K_{eq}}{K_{eq}+(1-K_{eq})e^{-\frac{v\delta}{D}}} \tag{4}$$

When measuring K as a function of the linear crystal growth rate at distinct mixing conditions, values D/δ and K_{eq} may be obtained by plotting $\ln(1/K-1)$ against v, giving a line with a slope of (δ/D) according to Sloan and McGhie.[26] v is the linear growth velocity of the ice formation (m s^{-1})

$$\ln\left(\frac{1}{K}-1\right)=\ln\left(\frac{1}{K_{eq}}-1\right)-\frac{v\delta}{D} \tag{5}$$

This is the so-called "Burton–Prim–Slichter" equation which was experimentally tested by several researchers, such as Burton et al.,[25] Zharinov et al.,[27] and Lionnet.[28] However, the experimental data were not extensive.

An idealized mathematical model of the distribution of solute between the liquid and solid phases during normal freezing of fixed volume sample was expressed by Pfann[29] and Baker[23]

$$\frac{C_i}{C_0}=K(1-g_f)^{K}-1 \tag{6}$$

where, g_f is the fraction that is frozen.

The model involves assumptions including the requirement of planar ice growth in the direction of freezing, no solute diffusion in the ice phase, complete mixing, and no density changes. These assumptions are not realistic for a practical system.

Two other basic distribution functions have been formulated for isomorphous impurity inclusion.[30–33] The distribution of the impurity between the liquid and the solid phases follows the relation (Berthelot–Nerst or the D-law)

$$\frac{C_1}{C_2}=K_D\frac{C_1{}^0-C_1}{C_2{}^0-C_1} \tag{7}$$

and (Doerner and Hoskins or the λ-law)

$$ln\frac{C_1{}^0}{C_1{}^0-C_1}=K_\lambda ln\frac{C_2{}^0}{C_2{}^0-C_2} \tag{8}$$

where, C_1^0 and C_2^0 are the initial concentrations of the two components in the solution, C_1 and C_2 are the amounts of them after a certain crystallization and K_D and K_λ are the distribution coefficients. Murthy and Mahadevappa[34] worked with the problem of fractional crystallization of two isomorphous salts of different molecular weights and concluded that both the D- and the λ-laws were not applicable to their systems. Their experimental results agreed, with the predictions of the Abu Elamayem equation; this equation applies to both equilibrium and nonequilibrium conditions. In the papers by Zhmurova et al.,[35,36] it was reported that the D-law holds over a wide range of concentrations and supersaturations (even under nonequilibrium conditions) for the isomorphic system studied. Nyvlt[33] pointed out that the D-law holds for both constant concentrations of the macrocomponent and the macrocomponent in the solution and the λ-law for a constant concentration of the macrocomponent and a variable concentration of macrocomponent in the solution. These models are more suited for bulk relationships rather than the interfacial and local. More importantly, none of these models, as they are, can accommodate the impacts of concentration, diffusive mass transfer, fluid-flow effect, and crystal growth rate when they are coupled together.

Distribution coefficient in practical systems

The effective distribution coefficients of solution and melt systems have been reported by some researchers such as Noll,[37] Hardy and Coriell,[38] Kirgintsev and Gorbacheva,[39] and Kirgintsev and Revzin.[40] Reid et al.[30,31] correlated that the effective distribution coefficient is dependent not only on the thermodynamic properties of the system, but operating variables such as temperature gradient and geometry as well. Liscom et al.[41] used an aqueous acetic acid solution and found that K decreases as solute concentration became more dilute. Baker[42] reported that K depends on rate of cooling, mixing, and composition of the original sample. Hurle[43] have shown that temperature fluctuations during the measurement of distribution coefficients by directional solidification tend to decrease the average degree of solidification.

Distribution coefficients for dilute concentration organic and inorganic aqueous solutions were investigated in a cooling rotating evaporator by Kobayashi and Lee[44] and Baker.[23,45–47] The freezing of seawater was studied by Foster,[48] Wakatsuchi and Ono,[49] and Brewster and Gebhart.[50] The water–ice interface salinity and the ice salinity were given as a function of ice growth rate. Mullier and Sekoulov[51] investigated the clearing efficiency of wastewater treatment by freezing concentration method using a falling film reactor. Mullier's experimental results show that variables

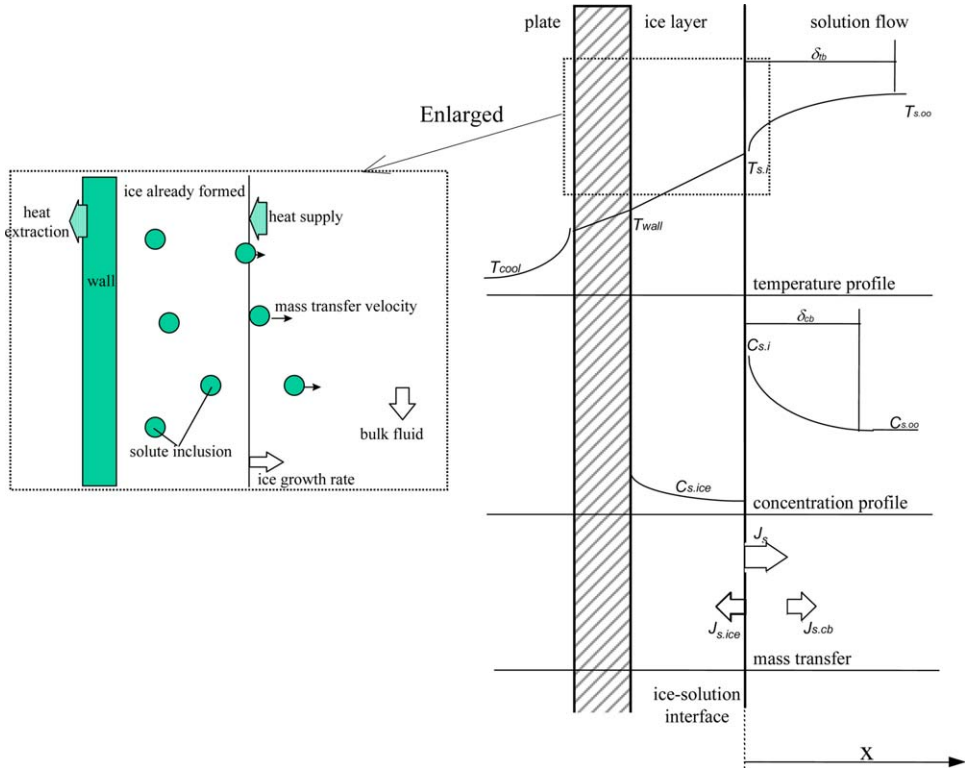

Figure 2. Schematic diagram of microscopic view of ice growth from solution flows.

[Color figure can be viewed in the online issue, which is available at wileyonlinelibrary.com.]

such as concentration of the solution, freezing rate, and internal mixing rates markedly affect the purification efficiency. Neumann and Ulrich[52] measured the effective distribution coefficient for caprolactam–cyclohexanone. The effect of flowing on the effective distribution coefficient could be seen. The primary investigation of purification of caprolaction–water, caprolaction–cyclohexanone, and dodecanole–decanole systems by suspension and layer crystallizations was carried out by Ulrich and Ozoguz,[53] Poschmann and Ulrich,[54] Henning and Ulrich,[55] and Ulrich and Neumann.[56]

For food liquids, Bayindirli et al.[57] reported distribution coefficients based on the average concentration of the solids in ice and liquid phases for apple juice freezing. They concluded that the solids distribution between the juice and ice was constant at constant freezing temperature. Mahmutoglu and Esin[58] measured the distribution coefficients at the interface for carrot juice at slow freezing rates at static conditions. Flesland[59] measured the average solute mass fraction in ice layers formed from falling films of sucrose solution from which coefficients were calculated and the relationship of the average distribution coefficients and the ratio of the ice growth rate to mass transfer coefficient was presented. For practical purposes, the average distribution coefficients as influenced by process conditions are the most important parameter.

Process visualization

The processes considered here are the processes of ice formation on steel plates from flowing solutions in channels or in falling films, which are shown in Figure 1b1 and Figure 1b2. Solution flows through the channel or over a plate at a certain velocity. Coolant flows extract heat from both sides (b1) of every solution channel or on one side (b2). Certainly the crystallizer geometries may not be only flat plates, it can be cylindrical as described by Hernańdez et al.[60] The discussion considered here is more of a flat plate geometry that can accommodate cylindrical cases, provided the crystal layer is thin compared with the system diameter.

Ice forms on the wall(s) cooled from the other side. For (b1), because the symmetrical nature, only half of the channel needs to be considered in this theoretical analysis. As soon as ice starts to form on the cooled surface, both temperature and concentration at the solid-liquid interface starts to change. It is known from literature[50,59] and the experimental results in the same laboratory by Chen,[61] that solute concentration in ice is always lower than that of the bulk solution, that is, $C_{\mathrm{s.ice}} < C_{\mathrm{s.}\infty}$. As the ice layer grows thicker, water molecules next to the ice-liquid interface become immobile. This "pushes" the solute molecules to move away from the ice-liquid interface, which increases solute concentration in the liquid side of the interface, that is, $C_{\mathrm{s,i}}$ becomes greater than $C_{\mathrm{s.}\infty}$. As this happens, the temperature at the interface must be reduced further to enable ice to form due to the freezing point depression (FPD) phenomena,[62] that is, the freezing temperature decreases due to the increasing $C_{\mathrm{s,i}}$.

Nevertheless, a common visualization of the above processes occurring at the solid-liquid interface (in either configuration Figure 1b1 or configuration Figure 1b2) is given in Figure 2.

Solute molecules on the liquid side of the interface is "pushed" into the bulk liquid because of the moving front of ice formation and, as shown in Figure 2, solute flux into liquid as pure ice forms is $J_{\mathrm{s}} = v_{\mathrm{ice}} C_{\mathrm{s,i}}$. This flux leads to an increase in $C_{\mathrm{s,i}}$, creating a concentration gradient between the ice-liquid interface and the bulk solution flow. This concentration gradient creates a concentration boundary layer

with certain thickness δ_{cb}. The mobile solute molecules are transported from the interface to solution flow by the concentration gradient near the interface in the solution side, that is

$$J_{s\,cb} = -D\left.\frac{\partial C}{\partial x}\right|_{x=0} \tag{9}$$

One can visualize that if $J_{s\,cb} \geq J_s$ solute would move away sufficiently fast that the solution near the interface is fully displaced by the ice moving front. If $J_{s\,cb} < J_s$, however, there would be some solute ($J_{s\,ice}$) retained by the ice. According to the mass balance, $J_s = J_{s\,cb} + J_{s\,ice}$. Hence, this process is an unsteady state heat and mass transfer process coupled with phase change. Based on this basic understanding, Chen and Chen[3] has developed a semiempirical model that correlates very well with the experimental average distribution coefficient

$$\bar{K} = a + b\mathrm{FPD} + c\mathrm{FPD}^2 + d\frac{\bar{v}_{ice}}{u_{s,\infty}{}^{0.5}} \tag{10}$$

with $a = -0.1$, $b = 0.32$, $c = -0.04$, and $d = 0.12$ for all the solutions tested by Chen.[61] These were sucrose solutions, whole milk, skim milk, orange juice, glycol solution, fructose solutions, NaCl solutions, and potato starch suspensions. The molecular influences on the entrapment or impurity inclusion are imbedded in the parameter FPD of the test solutions representing the bulk concentration effect. This empirical correlation has been found useful in the analysis of data from falling film FC as shown by Moreno et al.[63]

There has been, in recent time, an increasing interest in the area of layer crystallization, in both modes (b1) and (b1) as shown in Figure 1 though their geometry may vary. For instance, Jiang et al.[4] proposed an additive type effective (average) distribution coefficient function that considers the impurity trapping as being dependent upon the crystal network type/structure (with or without the branched-porous structure coexisting together). This function is intertwined with the ideal distribution coefficient of impurity i on the crystal-liquid interface, an effective distribution coefficient of impurity i in the branched porous structure, film temperature difference, and thickness of mass transfer boundary layer. Despite the advances made in segregating the mechanisms involved, these models tend to be much more complex than the one introduced here.

Here, we have started the analysis from the basic convection–diffusion mass transfer equation, and we have made some assumptions to progress to a set of simpler equations describing the average distribution coefficient. The focus has been on obtaining mass transfer correlations with more fundamental meaning yet preserving some kind of simplicity. Comprehensive experimental data available on both category (b1) and (b2) with a wide range of sucrose solutions have been used to validate the approach. Two solution routes have been taken showing similar trends. Their differences have been discussed as well.

Deriving New Formula of Average/Mean Distribution Coefficient

Governing equation for mass transfer

For simplicity, because the amount of ice formed from solution flow is comparatively small against the amount of flowing solution, the effect of ice formation on concentration distribution at different locations along the flow direction has been neglected. This has led to the assumption of a 1-D situation. Hence, the differential equation for mass transfer in the concentration boundary layer can be written as follows

$$\frac{\partial C}{\partial t} = \nabla \cdot (D\nabla C) - u_s \cdot \nabla C \tag{11}$$

Assuming the reference point is fixed at the ice/solution interface, that is, $u_{s.x} \approx -v_{ice}$ (Figure 2). Equation 11 can then be simplified to

$$\frac{\partial C}{\partial t} = \frac{\partial}{\partial x}\left(D\frac{\partial C}{\partial x}\right) + v_{ice}\frac{\partial C}{\partial x} \tag{11a}$$

This approach may be regarded as being analogous to modeling flat-plate membrane filtration.[64,65]

Concentration relationships

Mass concentration (C, kg/m^3) or molar concentration (C_m, mol/m^3) ($C = MC_m$) is commonly used in mass conservation equation. However, weight percentage (ω, wt %) is usually used for calculating the distribution coefficient K. Before analyzing the mathematical model (Eq. 11), it is useful to go through some definitions related to the distribution coefficient.

The distribution coefficient (K) is defined as

$$K = \frac{\omega_{s.ice}}{\omega_{s.\infty}} \tag{12}$$

For an aqueous solution, the following relationship exists

$$\frac{C_{H_2O}}{\rho_{H_2O}} + \frac{C_s}{\rho_s} = 1 \text{ or } C_{H_2O} = \rho_{H_2O} - C_s\frac{\rho_{H_2O}}{\rho_s} \tag{13}$$

The mass percentages $\omega_{s.ice}$ and $\omega_{s.\infty}$ can be written as

$$\omega_{s.\infty} = \frac{C_{s.\infty}}{C_{s.\infty} + C_{H_2O}} = \frac{C_{s.\infty}}{C_{s.\infty} + \rho_{H_2O} - \frac{\rho_{H_2O}}{\rho_s}C_{s.\infty}} \tag{14}$$

$$\omega_{s.ice} = \frac{C_{s.ice}}{C_{s.ice} + C_{H_2O}} = \frac{C_{s.ice}}{C_{s.ice} + \rho_{H_2O} - \frac{\rho_{H_2O}}{\rho_s}C_{s.ice}} \tag{15}$$

where Eq. 13 has been used.

Substituting Eqs. 14 and 15 into Eq. 12, the distribution coefficient can be expressed as

$$K = \frac{C_{s.ice}\left(C_{s.\infty} + \rho_{H_2O} - \frac{\rho_{H_2O}}{\rho_s}C_{s.\infty}\right)}{C_{s.\infty}\left(C_{s.ice} + \rho_{H_2O} - \frac{\rho_{H_2O}}{\rho_s}C_{s.ice}\right)} \tag{16}$$

Equation 16 can be rearranged to

$$C_{s.ice} = \frac{K\rho_{H_2O}C_{s.\infty}}{C_{s.\infty}(1-K)\left(1-\frac{\rho_{H_2O}}{\rho_s}\right) + \rho_{H_2O}} \tag{17}$$

In the above equations, all the concentration values in the ice layer are the average or the mean value (over the time period of ice formation). In the following sections, we present two approximate solutions of the pseudosteady nature.

Model A

Assuming the pseudosteady state, that is, $\frac{\partial C}{\partial t} \approx 0$, as the ice growth rate is very small (typically of several $\mu m\ s^{-1}$). In this case, the mass conservation Eq. 11a becomes

$$\frac{\partial}{\partial x}\left(D\frac{\partial C}{\partial x}\right)+v_{\text{ice}}\frac{\partial C}{\partial x}=0 \tag{18}$$

The boundary conditions are

$$C=C_{\text{s.}\infty}, \text{when } t\geq 0,\ x=\delta_{\text{cb}} \tag{19}$$

$$C=C_{\text{s.i}}, \text{when } t\geq 0,\ x=0 \tag{20}$$

$$-D\frac{\partial C}{\partial x}=v_{\text{ice}}(C_{\text{s.i}}-C_{\text{s.ice}}) \tag{21}$$

Integrating Eq. 18 once and applying the boundary conditions (Eqs. 20 and 21), one can obtain

$$D\frac{\partial C}{\partial x}=-v_{\text{ice}}(C-C_{\text{s.ice}}) \tag{22}$$

Integrating this equation against x, and for simplicity, we assume that the diffusivity D is a function of $T_{\text{s.}\infty}$ and $C_{\text{s.}\infty}$ only, one can further obtain

$$ln\frac{C_{\text{s.}\infty}-C_{\text{s.ice}}}{C_{\text{s.}i}-C_{\text{s.ice}}}=\text{e}^{-\frac{v_{\text{ice}}}{D/\delta_{\text{cb}}}}=\text{e}^{-\frac{v_{\text{ice}}}{\beta}} \tag{23}$$

Here the mass coefficient $\beta\approx\frac{D}{\delta_{\text{cb}}}$. Rearranging Eq. 23, one can write down

$$C_{\text{s.ice}}=\frac{C_{\text{s.}\infty}\left(1-\frac{C_{\text{s.i}}}{C_{\text{s.}\infty}}\text{e}^{-\frac{v_{\text{ice}}}{\beta}}\right)}{1-\text{e}^{-\frac{v_{\text{ice}}}{\beta}}} \tag{24}$$

Combining the above equation and Eq. 17, one can obtain

$$K=\frac{\left(1-\frac{C_{\text{s.i}}}{C_{\text{s.}\infty}}\text{e}^{-\frac{v_{\text{ice}}}{\beta}}\right)\left(C_{\text{s.}\infty}\left(1-\frac{\rho_{\text{H}_2\text{O}}}{\rho_{\text{s}}}\right)+\rho_{\text{H}_2\text{O}}\right)}{\left(1-\frac{C_{\text{s.i}}}{C_{\text{s.}\infty}}\text{e}^{-\frac{v_{\text{ice}}}{\beta}}\right)C_{\text{s.}\infty}\left(1-\frac{\rho_{\text{H}_2\text{O}}}{\rho_{\text{s}}}\right)+\rho_{\text{H}_2\text{O}}\left(1-\text{e}^{-\frac{v_{\text{ice}}}{\beta}}\right)} \tag{25}$$

Equation 25 is one relationship established this far on the effects of the ratio of ice growth rate to mass transfer coefficient (v_{ice}/β; which may be called a "transfer velocity ratio," i.e., how quickly the ice front moves compared with how quickly the fluid convectively removes the solute from the ice surface to the bulk liquid), the ratio of interfacial solute concentration ($C_{\text{s.i}}/C_{\text{s.}\infty}$) and the distribution coefficient (K) for ice growth processes from solution flows.

To pursue the correlation further, it is interesting to note that the interfacial solute concentration ratio ($C_{\text{s.i}}/C_{\text{s.}\infty}$), would actually be determined by the transfer velocity ratio and perhaps, an influence due to the ice structure that is formed (for instance, the "micro- or nanovoids" in between pure solid ice microdomains which allows the pools of solution of certain concentration to be staying).

If we think of the ice front as a "moving" permeable membrane, the solute penetration would be determined by both the cross-flow mass transfer, which "sweeps" the surface of the membrane to keep it clean. It is obvious that in this case, the amount of solute that can transfer through the membrane, or say can be trapped by the membrane pores, would be determined by the pore size and structure. It is thus envisaged that the material characteristics of the ice-moving front would play a significant role.

There is no analytical relationship available for $C_{\text{s.i}}/C_{\text{s.}\infty}$ as a function of v_{ice}/β and the material characteristics. It is too complex at this stage to consider quantitatively the effects of material characteristics. However, we can expect that $C_{\text{s.i}}$ depends on the ice growth rate, v_{ice}, and mass the mass transfer "velocity," β. In other words, the dimensionless quantity ($C_{\text{s.i}}/C_{\text{s.}\infty}-1$) would increase with the increasing velocity ratio v_{ice}/β. When $v_{\text{ice}}=0$, $C_{\text{s.i}}=C_{\text{s.}\infty}$. As a first approximation, we propose the following

$$\frac{C_{\text{s.i}}}{C_{\text{s.}\infty}}-1=\xi\frac{v_{\text{ice}}}{\beta} \tag{26}$$

where ξ is an empirical function, which may reflect well the impact of material characteristics. $C_{\text{s.}\infty}$ should affect $(\frac{C_{\text{s.i}}}{C_{\text{s.}\infty}}-1)$ no doubt, and therefore, a simple assumption here would be $\xi\sim {C_{\text{s.}\infty}}^{n}$. The relationship of $(\frac{C_{\text{s.i}}}{C_{\text{s.}\infty}}-1)$ vs. $\frac{v_{\text{ice}}}{\beta}$ then becomes

$$\frac{C_{\text{s.i}}}{C_{\text{s.}\infty}}-1=A_{\text{c}}{C_{\text{s.}\infty}}^{n}\frac{v_{\text{ice}}}{\beta} \tag{27}$$

The mass transfer coefficient (β), which can be calculated from available mass transfer correlations, together with the measured results of v_{ice}, we can plot the relationship between $(\frac{C_{\text{s.i}}}{C_{\text{s.}\infty}}-1)$ and ${C_{\text{s.}\infty}}^{n}\frac{v_{\text{ice}}}{\beta}$ with different n values. There are now two sets of experimental data we can use: the results for falling film crystallizer (FFC)[59] and the results for controlled flow suspension crystallizer (CFSC).[61] The calculations made on obtaining the mass transfer coefficients can be found in the Appendix.

When v_{ice}, $C_{\text{s}\cdot\text{ice}}$, and $C_{\text{s.}\infty}$ are known and β is determined by the aforementioned methods, $C_{\text{s.i}}$ can be determined from Eq. 23 by the expression below

$$C_{\text{s.i}}=\frac{C_{\text{s.}\infty}-C_{\text{s.ice}}\left(1-\text{e}^{-\frac{v_{\text{ice}}}{\beta}}\right)}{\text{e}^{-\frac{v_{\text{ice}}}{\beta}}} \tag{28}$$

Model B

Apart from the above Model A, it is also possible to twist somewhat the boundary condition set to allow the obtainment of the solution of the same governing Eq. 18 through the traditional boundary layer solution procedure.

The boundary conditions are:

$$C=C_{\text{s.}\infty}, \text{when } t\geq 0, x=\delta_{\text{cb}} \tag{29}$$

$$\frac{\partial C}{\partial x}=0, \text{when } t\geq 0, x=\delta_{\text{cb}} \tag{30}$$

$$C=C_{\text{s.i}}, \text{when } t\geq 0, x=0 \tag{31}$$

$$-D\frac{\partial C}{\partial x}=v_{\text{ice}}(C_{\text{s.i}}-C_{\text{s.ice}}) \tag{32}$$

Thus, there is one extra Eq. 29 that was added to the boundary condition set for Model A.

Based on the traditional approach in the theory of boundary layer transport,[66] one can assume the concentration profile fulfills a second-order polynomial fitting:

$$\frac{C_{\text{s.i}}-C}{C_{\text{s.i}}-C_{\text{s.}\infty}}=a_1+a_2\left(\frac{x}{\delta_{\text{cb}}}\right)+a_3\left(\frac{x}{\delta_{\text{cb}}}\right)^2 \tag{33}$$

The coefficients a_1, a_2, and a_3 can be determined

$$\frac{C_{\text{s.i}}-C}{C_{\text{s.i}}-C_{\text{s.}\infty}}=2\left(\frac{x}{\delta_{\text{cb}}}\right)-\left(\frac{x}{\delta_{\text{cb}}}\right)^2 \tag{34}$$

Based on these boundary conditions, one can arrive at an expression for $C_{\text{s,ice}}$

$$C_{s.ice} = C_{s.i} - \frac{2(C_{s.i} - C_{s.\infty})}{\frac{v_{ice}}{\beta}} \quad (35)$$

Combining Eqs. 17 and 35, one may eventually obtain a new expression of K

$$K = \frac{\left(2\left(1-\frac{C_{s.i}}{C_{s.\infty}}\right)+\frac{C_{s.i}}{C_{s.\infty}}\frac{v_{ice}}{\beta}\right)\left(C_{s.\infty}\left(1-\frac{\rho_{H_2O}}{\rho_s}\right)+\rho_{H_2O}\right)}{\left(2\left(1-\frac{C_{s.i}}{C_{s.\infty}}\right)+\frac{C_{s.i}}{C_{s.\infty}}\frac{v_{ice}}{\beta}\right)C_{s.\infty}\left(1-\frac{\rho_{H_2O}}{\rho_s}\right)+\rho_{H_2O}\frac{v_{ice}}{\beta}} \quad (36)$$

Similarly, the above equation can be coupled with Eq. 26 or more specially Eq. 27 (the empirical formula for interfacial solute concentration ratio) to yield an effective expression for the average/mean solute distribution coefficient K.

Results and Discussion

Manipulating the final analytical derivations in the aforementioned derivation section, two models of average/mean distribution coefficient (K) have been proposed here for both FFC and CSFC modes of operations.

Combining Eqs. 25 and 27, giving Model A

$$K = \frac{\alpha_1\left[C_{s.\infty}\left(1-\frac{\rho_{H_2O}}{\rho_s}\right)+\rho_{H_2O}\right]}{\rho_{H_2O}\left(1-e^{-\frac{v_{ice}}{\beta}}\right)+\alpha_1 C_{s.\infty}\left(1-\frac{\rho_{H_2O}}{\rho_s}\right)} \quad (37)$$

and

$$\alpha_1 = \left(1-e^{-\frac{v_{ice}}{\beta}}\right) - A_c {C_{s.\infty}}^n \frac{v_{ice}}{\beta} e^{-\frac{v_{ice}}{\beta}} \quad (38)$$

Combining Eqs. 36 and 27, giving Model B

$$K = \frac{\alpha_2\left[\rho_{H_2O}+C_{s.\infty}\left(1-\frac{\rho_{H_2O}}{\rho_s}\right)\right]}{\rho_{H_2O}+\alpha_2 C_{s.\infty}\left(1-\frac{\rho_{H_2O}}{\rho_s}\right)} \quad (39)$$

and

$$\alpha_2 = (1-2A_c {C_{s.\infty}}^n) + A_c {C_{s.\infty}}^n \frac{v_{ice}}{\beta} \quad (40)$$

Using the above equations, the constants (A_c and n) in the aforementioned two models for the two types of the crystallizers, respectively, can be determined by correlating the experimental data on average distribution coefficients. The calculated values are shown in Table 1.

The values of $(\frac{C_{s.i}}{C_{s.\infty}}-1)$ as a function of ${C_{s.\infty}}^n \frac{v_{ice}}{\beta}$ under different solution conditions have been plotted in Figures 3a, b for both FFC and CFSC's results using Model A. Similar plots, which are slightly more scattered (especially in the high velocity ratio region) have been made for Model B (Figures 4a, b). The numerical differences between the predicted and the experimental datasets were marginal between the two models. The values shown in Table 1 were the best correlations judging by the best r^2 attained as well as the observations made on the plots like that in Figure 3. It has been found that the values of $(\frac{C_{s.i}}{C_{s.\infty}}-1)$ and $\frac{v_{ice}}{\beta}$ are correlated well using Eq. 27 despite the simplicity of the approach. For CFSC, the power is $n = -0.31$ and for FFC the power is $n = -0.25$. Rounding them up using fractions, one may consider $n \approx -1/3$ for CSFC and $n \approx -1/4$ for FFC. These are consistent in both models, respectively.

To explore an interesting aspect of the process, to see if rather "pure" ice can be formed using this sort of process, some additional experiments were conducted and analyzed, for example, tests were done on 1.3 and 5 wt % sucrose solutions (Figure 5). The data points plotted in Figure 5 were obtained using the experimental procedures described previously. Each point represents a single experiment gained with the procedure that had ±4% relative error. The lines of average distribution coefficient against v_{ice}/β tends to intersect the $K = 0$ axis, meaning that rather pure ice can be formed from solution flows when ice grows at a rate, which is lower than the "critical" velocity ratio $(v_{ice}/\beta)^*$ at this intersection, that is, $K \approx 0$ for $v_{ice}/\beta < (v_{ice}/\beta)^*$. "*" denotes the critical value. Our experimental results indeed show that in these regions very pure ice can be formed, as shown by Chen and Chen et al.[61,67]

Table 1. The Model Constants in the for FFC and CFSC Valuated Using Model A and Model B

Crystallizer type	Concentration (wt %)	A_c	n	Model	r^2
FFC	10–40	4.50	−0.31	A	0.9807
CFSC	5–30	2.80	−0.25	A	0.9898
FFC	10–40	2.29	−0.31	B	0.9805
CFSC	5–30	1.43	−0.25	B	0.9834

From both Model A and Model B (Eqs. 25 and 36), respectively, the ice growth rates at the points of intersections can be found by setting $K = 0$, which are

$$\left(\frac{v_{ice}}{\beta}\right)^* = -ln\left(\frac{C_{s.\infty}}{C_{s.i}}\right) \text{ (Model A)} \quad (41)$$

$$\left(\frac{v_{ice}}{\beta}\right)^* = 2\left(1-\frac{C_{s.\infty}}{C_{s.i}}\right) \text{ (Model B)} \quad (42)$$

In those two solutions, $\left(\frac{v_{ice}}{\beta}\right)^* \geq 0$ because $C_{s.i} \geq C_{s.\infty}$. It may be considered that $\left(\frac{v_{ice}}{\beta}\right)^*$ is the maximum ratio of the ice growth rate, which is determined by heat transfer in the freezing process, to the mass transfer velocity below which quite pure ice can be formed under flow conditions. A comparison of the two solutions is given in Figure 6 in terms of $\left(\frac{v_{ice}}{\beta}\right)^*$ vs. $\frac{C_{s.i}}{C_{s.\infty}}$. It can be seen that when the concentration "gradient parameter" $\frac{C_{s.i}}{C_{s.\infty}}$ becomes greater than ~5, some departure can be observed between the two models though the general trends are similar.

From Eqs. 41 and 42, it can be seen that increasing mass transfer coefficient and decreasing the bulk concentration favor the increase of the maximum ice growth rate (thus higher freezing capacity) to assist pure ice formation. One of the methods to increase the mass transfer coefficient is to increase bulk solution velocity. The experimental results presented previously have already shown the effect of solution velocity on the average distribution coefficient, that is, increasing the solution velocity is effective in increasing the purity of ice formed from solution flows.[61,67] The experimental results were also obtained using 1.3 wt % sucrose solution. The lowest value of solute inclusion in ice has been found to be about 30 ppm from 1.3 wt % sucrose solution flow in the two parallel plate channel.[61]

From Eq. 41, for Model A, one can obtain

$$e^{\left(\frac{v_{ice}}{\beta}\right)^*} = \left(\frac{C_{s.i}}{C_{s.\infty}}\right) \text{ (Model A)} \quad (43)$$

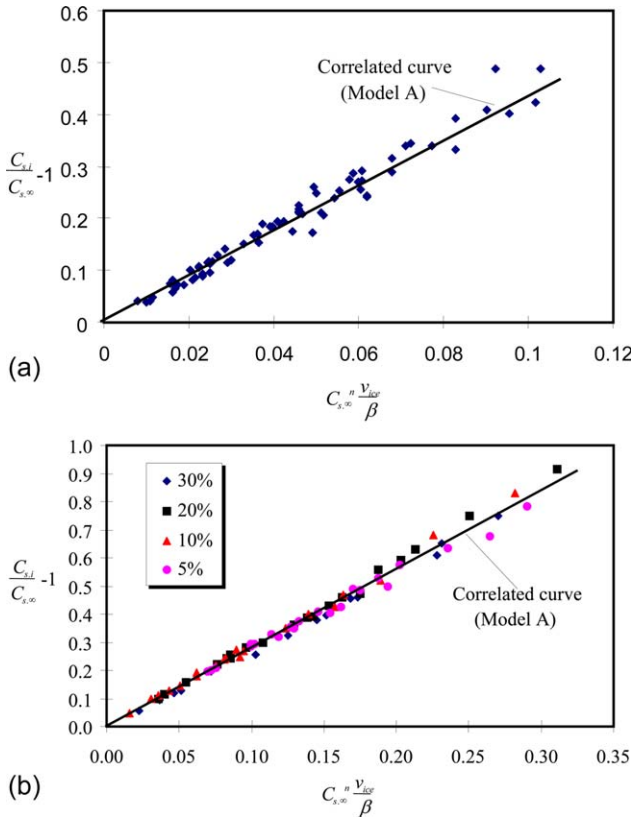

Figure 3. (a) ($C_{s,i}/C_{s,\infty}-1$) as function of $C_{s,\infty}{}^{n}\ v_{ice}/\beta$ ($n=-0.31$) for the experimental results of ice growth from falling film of sucrose solution (Model A). (b) ($C_{s,i}/C_{s,\infty}-1$) as function of $C_{s,\infty}{}^{n}\ v_{ice}/\beta$ ($n=-0.25$) for the experimental results of ice growth from sucrose solution flow in a CFSC channel (Model A).

[Color figure can be viewed in the online issue, which is available at wileyonlinelibrary.com.]

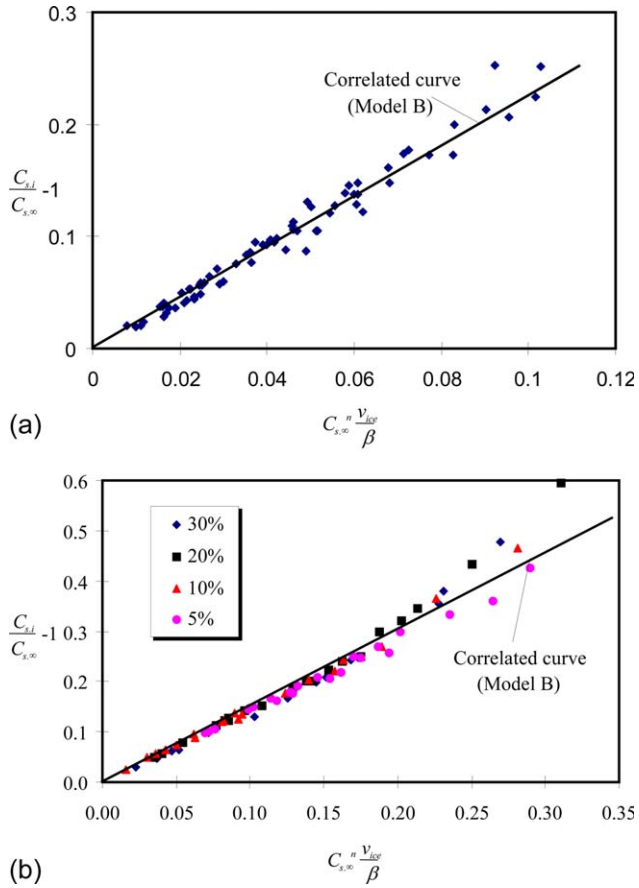

Figure 4. (a) ($C_{s,i}/C_{s,\infty}-1$) as function of $C_{s,\infty}{}^{n}\ v_{ice}/\beta$ ($n=-0.31$) for the experimental results of ice growth from falling film of sucrose solution (Model B). (b) ($C_{s,i}/C_{s,\infty}-1$) as function of $C_{s,\infty}{}^{n}\ v_{ice}/\beta$ ($n=-0.25$) for the experimental results of ice growth from sucrose solution flow in a CFSC channel (Model B).

[Color figure can be viewed in the online issue, which is available at wileyonlinelibrary.com.]

By combining Eqs. 27 and 43, for Model A, one can work out the critical velocity ratio as a function of the bulk concentration of the solution

$$C_{s,\infty}{}^{-n}=\frac{A_c\left(\frac{v_{ice}}{\beta}\right)^*}{e^{\left(\frac{v_{ice}}{\beta}\right)^*}-1} \tag{44}$$

From Eq. 42, for Model B, one can obtain

$$\frac{1}{1-\frac{1}{2}\left(\frac{v_{ice}}{\beta}\right)^*}=\left(\frac{C_{s,i}}{C_{s,\infty}}\right)\text{(Model B)} \tag{45}$$

By combining Eqs. 27 and 45, for Model B, one can work out the critical velocity ratio as a function of the bulk concentration of the solution

$$C_{s,\infty}{}^{-n}=2A_c\left[1-\frac{1}{2}\left(\frac{v_{ice}}{\beta}\right)^*\right] \tag{46}$$

Thus an interesting plot can be made for critical velocity ratio $\left(\frac{v_{ice}}{\beta}\right)^*$ vs. $C_{s,\infty}^{-n}$ $(-n>0)$ with Eqs. 44 and 46. This is shown in Figure 7 where $n=-0.25$. It is shown that Model B becomes unreasonable as the velocity ratio becomes higher as the bulk concentration gets to below zero, which is not intuitive. This is most likely due to the approximation formula made for the concentration distribution in the conventional boundary layer theory.

In general, when ice grows from a lower solute concentration solution, a larger solute concentration difference between

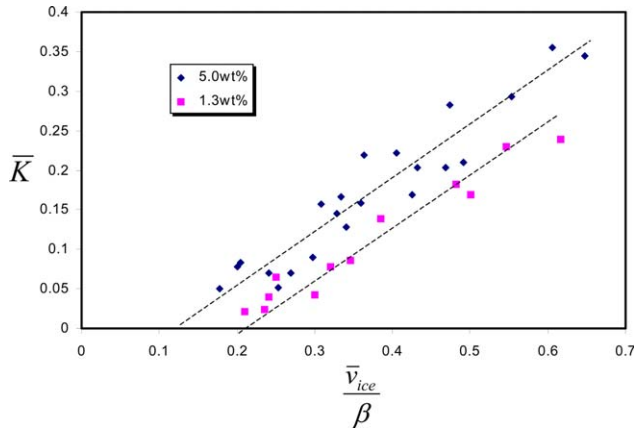

Figure 5. Average distribution coefficient vs. v_{ice}/β for 1.3 and 5 wt % sucrose solutions.

[Color figure can be viewed in the online issue, which is available at wileyonlinelibrary.com.]

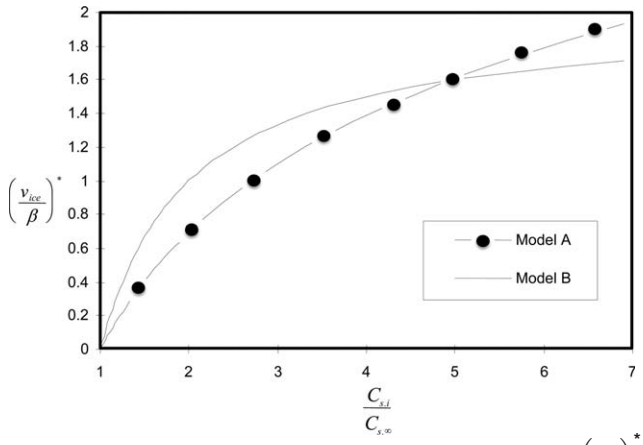

Figure 6. A comparison of the two solutions of $\left(\frac{v_{ice}}{\beta}\right)^*$ vs. $\frac{C_{s,i}}{C_{s,\infty}}$ given by Models A and B.

ice-solution interface and solution flow is created, which drives more solute molecules near the interface through the concentration boundary layer. A lower concentration solution is also of lower viscosity, which facilitates mass transfer. With lower bulk concentration of solute, pure ice could be made at a higher velocity ratio as shown in Figure 7.

It may also be interesting to use the above-developed model to look at what may happen in the static crystallization process (growth of crystal layer without deliberate stirring or fluid circulation) as those investigated by Kim and Ulrich.[68] To do that, the first approximation would be to invoke a mass transfer coefficient $\beta_{\text{diffusion}}$ with a transport characteristic length for diffusion-only process ($\delta_{\text{c,diffusion}}$) as follows

$$\beta_{\text{diffusion}} = \frac{D}{\delta_{\text{c,diffusion}}} \tag{47}$$

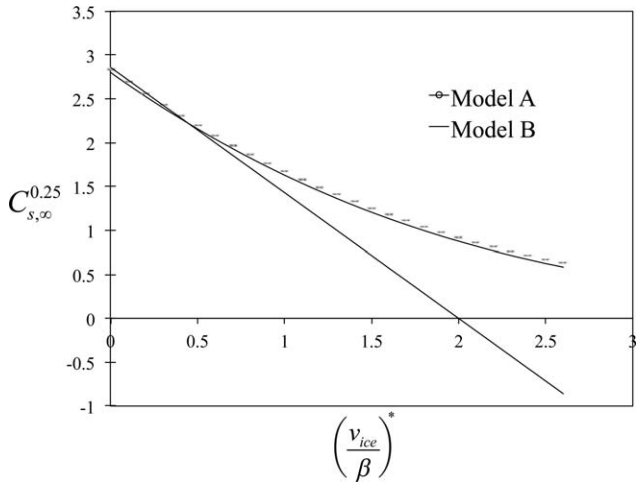

Figure 7. The relationship between the solute bulk concentration and velocity ratio (based on Model A and Model B); this shows that the validity of Model B ceases as bulk concentration increases to beyond the velocity ratio of about 2; as the velocity ratio goes up, Model A gives more meaningful projection, for instance as bulk concentration goes towards zero, the ice growth velocity can be made very high through freezing devices.

D is the mass diffusivity of the species in solution. Kim and Ulrich[68] provided the governing equation set of a layer crystallization system involving an energy balance and a mass balance, which was incorporated with interfacial boundary conditions, that is, movement of mass due to crystallization front development balanced with mass diffusion, as well as an interfacial solute concentration set to be dependent on the interfacial temperature, and a crystal growth rate (velocity) model. The equation set was numerically solved for a number of useful parameters including the interfacial distribution coefficient as the outcome of the computation. In this work, in contrast, we have correlated analytically the distribution coefficient in a flow system, which would be very useful as the interfacial condition for mass transfer modeling during FC.

Conclusions

In this article, two analytical models of solute inclusion level in ice as functions of ice growth rate (v_{ice}), mass transfer coefficient (β), solution concentration at interface ($C_{\text{s,i}}$) and bulk solution concentration ($C_{\text{s},\infty}$) under flow conditions, have been derived. The predicted average distribution coefficients agree well with the experimental results for both controlled suspension flow crystallizer and the FFC. The criteria for "pure ice" formation have also been investigated and the evidence of producing pure ice is reflected through the model formulation. Model A has been found to be more appropriate compared with Model B. Model A as provided in this study, should be quite useful in setting up the mass transfer boundary conditions for detailed numerical simulation of FC in future. It is also in a helpfully simple format that can assist in the "back of envelope calculation" about the phenomena hence it must be useful for equipment design.

Acknowledgments

The experimental data were obtained in the laboratory led by XDC during his time as a Professor at the Department of Chemical and Materials Engineering, The University of Auckland, New Zealand (1993-2006). Dr. Ping Chen was the PhD student, supervised by XDC, who conducted the detailed experimental work at the end of the last century.

Literature Cited

1. Rahman MS, Ahmed M, Chen XD. Freezing-melting process in liquid food concentration, Chapter 27. In: Rahman MS, editor. *Handbook of Food Preservation*, 2nd ed., Boca Raton: CRC Press, 2007: 667–690.
2. Chen P, Chen XD, Free K. An experimental study on the spatial uniformity of solute inclusion in ice formed from falling film flows on a sub-cooled surface. *J Food Eng*. 1999;39:101–105.
3. Chen P, Chen XD. A generalized correlation for solute inclusion in ice formed from aqueous solutions and food liquids on sub-cooled surface. *Can J Chem Eng*. 2000;78:312–319.
4. Jiang X, Hou B, He G, Wang J. Falling film melt crystallization (I): model development, experimental validation of crystal layer growth and impurity distribution process. *Chem Eng Sci*. 2012;84:120–133.
5. Jiang X, Hou B, He G, Wang J. Falling film melt crystallization (II): model to simulate the dynamic sweating using fractal porous media theory. *Chem Eng Sci*. 2013;91:111–121.
6. Zhou L, Su M, Benyahia B, Singh A, Parton PI, Trout BL, Myerson AS, Braatz RD. Mathematical modeling and design of layer crystallization in a concentric annulus with and without recirculation. *AIChE J*. 2013;59(4):1308–1321.

7. Rahman MS, Ahmed M, Chen XD. Freezing-melting process and desalination: I. Review of the state-of-the-art. *Sep Purif Rev*. 2006; 35:59–96.
8. Williams PM, Ahmad M, Connolly BS. Freeze desalination: an assessment of an ice maker machine for desalting brines. *Desalination*. 2013;308:219–224.
9. Attia A. New proposed system for freeze water desalination using auto reversed R-22 vapor compression heat pump. *Desalination*. 2010;254:179–184.
10. Boaventura BCB, Murakami ANN, Prudêncio ES, Maraschin M, Murakami FS, Amante ER, Amboni R. Enhancement of bioactive compounds content and antioxidant activity of aqueous extract of mate (Ilex paraguariensis A. St. Hil.) through freeze concentration technology. *Food Res Int*. 2012;53(2):686–692.doi:10.1016/j.foodres.2012.07.042.
11. Okawa S, Ito T, Saito A. Effect of crystal orientation on freeze concentration of solutions. *Int J Refrig*. 2009;32:246–252.
12. Tiller WA. *Principles of Solidification in the Art and Science of Growing Crystals*. New York: Wiley, 1963.
13. Brice JC. *The Growth of Crystals from the Melt*. Amsterdam, Holland: North-Holland Publishing Company, 1965.
14. Brice JC. *The Growth of Crystals from Liquid*. Amsterdam, Holland: North-Holland Publishing Company, 1973.
15. Arkenbout GJ. *Melt Crystallization Technology*. USA: Technomic Publishing Company, 1995.
16. Kitaigorodskll AI. *Molecular Crystal and Molecules*. New York: Academic, 1973;94–105.
17. Chernov AA. Excess impurity trapping during crystal growth. In: *Growth of Crystals*, New York: Consultans Bureau, 1962;3:35.
18. Chernov AA, Lyubov and Ya B. Growth theory and general aspects of single-crystal formation. In: *Growth of Crystals*. New York: Consultants Bureau, 1968;5A:7.
19. Chernov AA. Crystallization of binary systems as a random walk problem. *J Phys Chem Solids* 1967;Supplement No.1:25.
20. Baralis G. Distribution coefficients during the solidification of an ideal binary system in the presence of heat flow. *J Cryst Growth*. 1968;3/4:627–632.
21. Baur IH. Dynamics of melting and crystallization in mixtures. *Berichte Bunsengesellschaft fuer Phys Chem*. 1967;71:703.
22. Kirwan DJ, Pigford RL. Crystallization kinetics of pure and binary melts. *AIChE J*. 1969;15:442–449.
23. Baker RA. Trace organic contaminant concentration by freezing—III, ice washing. *Water Res*. 1969;3:717–730.
24. Chernov AA. *Modern Crystallography III—Crystal Growth*. Berlin, Germany: Springer-Verleg, 1984.
25. Burton JA, Prim RC, Slichter WP. The distribution of solute in crystals growth from the melt. Part I. *Theoret J Chem Phys*. 1953;21: 1987–1990.
26. Sloan GJ, McGhie AR. *Techniques of Melt Crystallization*. New York: Wiley, 1988.
27. Zharinov VI, Konovalov EE, Peizulaev SI and Kayurova TV. Concentration variation of the partition coefficient in the directed crystallization of aqueous sodium chloride solutions. *Russ J Phys Chem*. 1974;48(4):572–574.
28. Lionnet GRE. An interfacial model for the transfer of impurities into the sucrose crystal. *Trans IChemE*. 1998;76(A):803–808.
29. Pfann WG. *Zone Refining*, 2nd ed. New York: Wiley, 1966.
30. Reid RC, Botsaris GD, Margolis G, Kirwan DJ, Denk EG, Ersan GS, Tester J and Wong F. Crystallization—part I. Transport phenomena of nucleation and crystal growth. *Ind Eng Chem*. 1970; 62(11):52–67.
31. Reid RC, Botsaris GD, Margolis G, Kirwan DJ, Denk EG, Ersan GS, Tester J and Wong F. Crystallization—part II. Crystallization processes. *Ind Eng Chem*. 1970;62(12):148–155.
32. Nyvlt J. *Solid-Liquid Phase Equilibrium*. Prague: Elsevier and Academia Press, 1977.
33. Nyvlt J. *Industrial Crystallisation—The State of the Art*, 2nd ed., Weinheim, Germany: Verlag Chemie GmbH, 1982.
34. Murthy ASA, Mahadevappa DS. Distribution of isomorphous salts between aqueous and solid phases in fractional crystallization. *Aust J Chem*. 1969;22:2017–2020.
35. Zhmurova ZI, Khaimov-Mal'kov Ya V. Dependence of the distribution of an impurity on growth rate during the crystallization of isomorphic systems from solution. *Sov Phys Crystallogr*. 1970;15:108–111.
36. Zhmurova ZI, Khaimov-Mal'kov Ya V. Distribution of isomorphic impurities during crystallization from aqueous solution. *Sov Phys Crystallogr*. 1970;15:112–115.
37. Noll G. Segregation of ammonium fluoride into ice single crystals—physical ice, In: *Proceedings of 3rd International Symposium*. 1968; 113–119.
38. Hardy SC, Coriell SR. Morphological stability of cylindrical ice crystals. *J Cryst Growth*. 1969;5(5):329–337.
39. Kirgintsev AN, Gorbacheva II. Distribution of impurities during the directed crystallization of Tin. Investiya Sibirskogo Otdeleniye. *Akad Nauk SSSR Seriya Khim Kikh Nauk*. 1969;2:30–34.
40. Kirgintsev AN, Revzin GE. Distribution coefficients for some impurities during directed crystallization of tellurium. Investiya Sibirskogo Otdeleniye. *Akad Nauk SSSR Seriya Khim Kikh Nauk*. 1969;2:35–38.
41. Liscom PW, Jackson RW, Powers JE. Factors influencing achieved during normal freezing. *AIChE J*. 1967;13:90–104.
42. Baker RA. Microchemical contaminants by freeze concentration and gas chromatography. *J Water Pollut Control Fed*. 1965;37:1164–1170.
43. Hurle DTJ. Effects of fluctuation on the measurement of distribution coefficients by directional solidification. *J Cryst Growth*. 1969;5(4): 227–232.
44. Kobayashi S, Lee GF. Freeze concentration of dilute aqueous solutions. *Anal Chem*. 1964;36:2197–2198.
45. Baker RA. Trace organic contaminant concentration by freezing—I. Low inorganic aqueous solutions. *Water Res*. 1967;1:66–77.
46. Baker RA. Trace organic contaminant concentration by freezing—II. Inorganic aqueous solutions. *Water Res*. 1967;1:97–113.
47. Baker RA. Trace organic contaminant concentration by freezing—IV. Ionic effects. *Water Res*. 1970;4:559–573.
48. Foster TD. Experiments on haline convection included by the freezing of seawater. *J Geophys Res*. 1969;74(6):6967–6974.
49. Wakatsuchi M, Ono N. Measurements of salinity and volume of brine excluded from growing sea ice. *J Geophys Res*. 1983;88(C5): 2943–2951.
50. Brewster RA, Gebhart B. The effects of supercooling and freezing on natural convection in seawater. *Int J Heat Mass Transf*. 1994; 37(4):543–552.
51. Muller M, Sekoulov I. Waste water reuse by freeze concentration with a falling film reactor. *Water Sci Technol*. 1992;26(7–8):1475–1482.
52. Neumann M, Ulrich J. Progressive freezing process. In: Rojkowski Z, editor, *Proceedings of the 12th Symposium on Industrial Crystallization*. Warsaw, Poland, September 21–23, 1993:1.061–1.066.
53. Ulrich J, Ozoguz Y. Progressive freezing and sweating in a test unit. *J Cryst Growth*. 1990;99:1134–1137.
54. Poschmann M, Ulrich J. Fractional suspension crystallization with additional purification steps. *J Cryst Growth*. 1996;167:248–252.
55. Henning S, Ulrich J. Description of the migration of liquid inclusions in growing crystallization layers. *Trans IChemE*. 1997;75(A): 233–236.
56. Ulrich J, Meumann M. Purification by solid layer melt crystallization. *J Therm Anal*. 1997;48:527–533.
57. Bayindirli L, Ozilgen M, Ungan S. Mathematical analysis of freeze concentration of apple juice. *J Food Eng*. 1993;19:95–107.
58. Mahmutoglu T, Esin A. Distribution coefficients at the interface for carrot juice at slow freezing rates. *J Food Eng*. 1996;27:291–295.
59. Flesland O. Freeze concentration by layer crystallization. *Drying Technol*. 1995;13(8&9):1713–1739.
60. Hernańdez E, Raventós M, Auleda JM, Ibarz A. Concentration of apple and pear juices in a multi-plate freeze concentrator. *Innov Food Sci Emerg Technol*. 2009;10:348–355.
61. Chen P. Freeze concentration of food liquids using layer crystallizers. PhD thesis, Dept. of Chemical and Materials Engineering, The University of Auckland, *New Zealand*. 1999.
62. Wolf AV, Brown MG, Prentiss PG. Concentrative properties of aqueous solutions: conversion table. In: Weast RC, Astle MJ, editors, *CRC Handbook of Chemistry and Physics*, 63rd ed. Florida: CRC Press, 1982.
63. Moreno FL, Raventós M, Hernańdez E, Ruiz Y. Behaviour of falling-film freeze concentration of coffee extract. *J Food Eng*. 2014;141:20–26.
64. Leung WF, Probstein RF. Low polarization in laminar ultrafiltration of macromolecular solution. *Ind Eng Chem Fundam*. 1979;18(3): 274–278.
65. De S, Bhattacharya PK. Prediction of mass-transfer coefficient with suction in the applications of reverse osmosis and ultrafiltration. *J Membr Sci*. 1997;128:119–131.

66. Incropera FP, DeWitt DP, Bergman TL, Lavine AS. *Introduction to Heat Transfer*. New York: Wiley, 2006.
67. Chen P, Chen XD, Free K. Solute inclusion in ice formed from sucrose solutions on a sub-cooled surface—an experimental study. *J Food Eng*. 1998;38:1–13.
68. Kim K, Ulrich J. Impurity distribution in a solid-liquid interface during static layer crystallization. *J Colloids Interface Sci*. 2002;252: 161–168.
69. Wilker W. *Warmeubergang an Rieselfilme*, VDI-Forschungsheft 490, Dusseldorf: VDI Verlag, 1962.
70. Shah RK, London AL. Laminar flow forced convection in ducts—a source book for compact heat exchanger analytical data. In: *Advances in Heat Transfer, supplement 1*. New York: Academic Press, 1978.
71. Cussler EL. *Diffusion, Mass Transfer in Fluid System*. Cambridge, New York: Cambridge University Press, Co., 1984.
72. Tyrrel HJV, Harris KR. *Diffusion in Liquids*. London: Butterworths, 1984.
73. Keppeler RA, Boose JR. Thermal properties of frozen sucrose solution. *Trans ASAE,* 1970;13:335–339.
74. Liley E P, Reid RC, Buck E. Physical and chemical data. In: Perry RH, Green DW, editors. *Perry's Chemical Engineering Handbook, 60th ed*. Singapore: McGraw-Hill, 1984:3–254.

APPENDIX 1: CALCULATIONS OF THE MASS TRANSFER COEFFICIENTS

(i) Calculation of β for FFC

Flesland[59] determined the mass transfer coefficient (β) for each condition of his experimental data on a FFC according to the Wilker's correlation.[69] *Re* can be calculated by

$$Re=\frac{G_{\mathrm{ff}}}{\mu b_{\mathrm{ff}}} \tag{A1}$$

where, G_{ff} is the mass flow, ρ is the density of the solution, μ is the dynamic viscosity, and b_{ff} is the width of the film.

The film thickness (δ) is calculated from the equations below

$$\delta=\left(\frac{3\nu^2}{g}\right)^{\frac{1}{3}}Re^{\frac{1}{2}}(Re<400) \tag{A2}$$

$$\delta=0.302\left(\frac{3\nu^2}{g}\right)^{\frac{1}{3}}Re^{\frac{8}{15}}(\mathrm{Re}>400) \tag{A3}$$

where g is the gravity acceleration.

For the FFC, the *Nu* correlations were given by Wilker[69] as the following

$$Nu=1.88\ \ Re<Re_{\mathrm{t}} \tag{A4}$$

$$Nu=0.0614Re^{\frac{8}{15}}Pr^{0.344}\ \ Re_{\mathrm{t}}<Re<\ 400 \tag{A5}$$

$$Nu=0.00112Re^{\frac{5}{6}}Pr^{0.344}\ \ 400\ <Re<\ 800 \tag{A6}$$

$$Nu=0.0066Re^{\frac{14}{15}}Pr^{0.344}\ \ Re>\ 800 \tag{A7}$$

where the transitional Reynolds number is

$$Re_{\mathrm{t}}=615Pr^{-0.646} \tag{A8}$$

For the mass transfer calculations, the analogy to heat transfer is applied and *Nu* is replaced by *Sh* and *Pr* by *Sc*. Then, the mass transfer coefficient (β) can be calculated

$$\beta=\frac{Sh\cdot D}{\delta_{\mathrm{cb}}} \tag{A9}$$

(ii) Calculation of β for CFSC

Determination of the Sherwood Number of the Flow in CFSC. The flow in CSFC has the H1 boundary condition similar to that defined by Shah and London.[70] Shah and London gave the mean *Nu* number (Nu_{ave}) with the H1 boundary condition as a function of the aspect ratio of rectangular channel (α_{e}) and axial coordinate for the thermal entrance region ($x_{\mathrm{e}}=Re\ Pr\ x\ /\ d_{\mathrm{h}}$). *Nu* can be replaced by *Sh* under the same flow and thermal conditions due to the analogy between the heat and mass transfer. The relationship for mass transfer is

$$\begin{aligned}Sh_{\mathrm{ave}}=&6.4780+0.1353\left(\frac{1}{x_{\mathrm{e}}}\right)-0.00113\left(\frac{1}{x_{\mathrm{e}}}\right)^2\\&-5.586\alpha_{\mathrm{e}}+3.0085(\alpha_{\mathrm{e}})^2+0.02013\left(\frac{\alpha_{\mathrm{e}}}{x_{\mathrm{e}}}\right)\end{aligned} \tag{A10}$$

Determination of the Diffusion Coefficient. The diffusion coefficient may be predicted by the following equation[71]

$$D=\frac{\left(\frac{R}{N_{\mathrm{m}}}\right)T}{6\pi vs} \tag{A11}$$

Another method of predicting liquid diffusivity, is[71]

$$D=0.124\times10^{-16}\left(\frac{RT}{\mu}\right)\left(\frac{(V_{\mathrm{c}})^{\frac{2}{3}}}{V}\right) \tag{A12}$$

Both equations retain the simple temperature and viscosity dependence of the Stokes–Einstein equation

$$D=\psi\frac{T}{v}=\psi\frac{T\rho}{\mu} \tag{A13}$$

where ψ is a constant, which may be determined using the diffusion coefficient of the dilute solution (D_{dil}). For dilute sucrose solution at 25°C, $D_{\mathrm{dil}}=1\times10^{-9}$ m^2/s.[72] The D of sucrose solution of different concentrations at various temperatures can then be calculated using the density data[73] and kinematic viscosity data.[74] Note here D is a function of $T_{\mathrm{s},\infty}$ and $C_{\mathrm{s},\infty}$.

The mass transfer coefficient (β) can then be determined using the correlation for *Sh* (Eq. A10) and *D* (Eq. A13)

$$\beta=\frac{Sh\cdot D}{d_{\mathrm{h}}} \tag{A14}$$

where d_{h} is the hydraulic diameter of the actual duct/channel.

Manuscript received Sep. 2, 2014, and revision received Nov. 25, 2014.